ADVANCED ENERGY MATERIALS
www.advenergymat.de

Influence of Processing Parameters and Molecular Weight on the Morphology and Properties of High-Performance PffBT4T-2OD:$PC_{71}BM$ Organic Solar Cells

Wei Ma, Guofang Yang, Kui Jiang, Joshua H. Carpenter, Yang Wu, Xiangyi Meng, Terry McAfee, Jingbo Zhao, Chenhui Zhu, Cheng Wang, Harald Ade,* and He Yan**

The influences of various processing parameters and polymer molecular weight on the morphology and properties of poly[(5,6-difluoro-2,1,3-benzothiadiazol-4,7-diyl)-alt-(3,3‴-di(2-octyldodecyl) 2,2′;5′,2″;5″,2‴-quaterthiophen-5,5‴-diyl)] (PffBT4T-2OD)-based polymer solar cells (PSCs) are investigated. High spin rate/high temperature conditions are found to significantly reduce polymer crystallinity and change polymer backbone orientation from face-on to edge-on. Most surprisingly, it is found that the median domain sizes of PffBT4T-2OD:PC71BM blends processed at different temperatures/spin rates are nearly identical, while the average domain purity and the molecular orientation relative to polymer:fullerene interfaces can be significantly changed by the processing conditions. A systematic study is carried out to identify the roles of individual processing parameters including processing temperature, spin rate, concentration, and solvent mixtures. Furthermore, the effect of molecular weight on morphology control is also examined. These detailed studies provide important guidance to control and optimize various morphological parameters and thus electrical properties of PffBT4T-2OD-type materials for the application in PSC.

1. Introduction

Polymer solar cells (PSCs) have attracted considerable attention in recent years due to their low cost, light weight, flexibility, simple preparation requirements, semitransparency, and their potential for large-area fabrication.[1–4] Bulk heterojunction (BHJ) PSCs based on interpenetrating networks of semiconducting polymers and fullerene derivatives have shown power conversion efficiencies (PCEs) >10%[3,5] for single layer devices and >11%[6] for tandem cells. The current BHJ paradigm conjectures an ideal morphology involving a bicontinuous network consisting of small domains ≈10–20 nm in size, sufficiently pure phases, a high degree of aggregation/crystallinity, and face-on orientation with respect to the substrate as well as the donor/acceptor (D/A) interface, thus improving charge dissociation and charge transport efficiency.[7–26] Controlling processing conditions to achieve a morphology close to the ideal is as important as synthesis of new donor and acceptor materials, and has become one of the main focus areas in PSC research.[27] In particular, controlling the conditions during spin-coating by using different solvents, mixed solvents, and/or additives[12,16,17,20–22,28–32] and after spin-coating by using thermal annealing, solvent annealing, solvent treatments, and light processing[11,33–35] has been widely investigated. It is also considered that the initial preaggregation state of the blend in solution has a critical impact on the final BHJ structure,[36,37] and the details of structure and morphology creation during casting are being increasingly investigated with time-resolved experiments.[38,39] Recently, an important approach of morphology control was demonstrated by utilizing the temperature-dependent aggregation property of the polymer in solution and that led to an open literature record device performance (10.8%) based on a polymer named poly[(5,6-difluoro-2,1,3-benzothiadiazol-4,7-diyl)-alt-(3,3‴-di(2-octyldodecyl) 2,2′;5′,2″;5″,2‴–quaterthiophen-5,5‴-diyl)] (PffBT4T-2OD).[3] PffBT4T-2OD is a very promising, high-performance conjugated polymer yielding PCEs up to 10.8% for a single junction polymer solar cell. The material has several intriguing characteristics:[3] (a) Unlike other high-performance

Prof. W. Ma, G. Yang, Y. Wu, X. Meng
State Key Laboratory for Mechanical Behavior of Materials
Xi'an Jiaotong University
Xi'an 710049, China
E-mail: msewma@mail.xjtu.edu.cn
G. Yang, K. Jiang, J. Zhao, Prof. H. Yan
Department of Chemistry
Hong Kong University of Science and Technology
Clear Water Bay, KowLoon, Hong Kong
E-mail: hyan@ust.hk
J. H. Carpenter, T. McAfee, Prof. H. Ade
Department of Physics
North Carolina State University
Raleigh, NC 27695, USA
E-mail: harald_ade@ncsu.edu
Dr. C. Zhu, Dr. C. Wang
Advanced Light Source
Laurence Berkeley National Laboratory
Berkeley, CA 94720, USA

DOI: 10.1002/aenm.201501400

materials,[13,40,41] PffBT4T-2OD can perform well with several fullerenes, i.e., four PffBT4T-2OD:fullerene combinations yield devices with PCE > 10%; (b) PffBT4T-2OD shows high hole mobility ($1.5–3.0 \times 10^{-2}$ cm^2 V^{-1} s^{-1}) in the blend; and (c) PffBT4T-2OD based blends exhibit high performance and high FF (>75%) even in thick films (≈300 nm). The morphology forming process of PffBT4T-2OD based blends is particularly interesting because PffBT4T-2OD shows strong temperature-dependent aggregation property in solution, which was utilized to create the near-ideal polymer:fullerene morphology containing highly crystalline and pure yet reasonably small polymer domains.[3]

To understand the aggregation and morphology properties of PffBT4T-2OD in details and fully explore the potential of this material, it is important to understand how various processing parameters affect the detailed morphology parameters of the PffBT4T-2OD-based blends including polymer crystallinity, backbone orientation, domain size, domain purity, and molecular orientations at D/A interfaces. Moreover, casting from hot solvents remains somewhat of an art and the impact of experimental protocols of hot solutions in general and PffBT4T-OD in particular have yet to be delineated carefully. The details of the morphology formed from PffBT4T-OD blends when casting from different solution temperatures and spin rates remain unknown. Furthermore, the impact of the molecular weight (M_w) is considered to be critical on morphology control and final device performance.[42] The M_w impact of PffBT4T-2OD on the aggregation properties and temperature sensitivity of morphology formation is also poorly understood and needs to be explored.

In this paper, we report a detailed study on the influence of various processing parameters and polymer molecular weights on the morphology of PffBT4T-2OD based devices. In order to clearly demonstrate the morphological effects of spin rate and processing temperatures, we have combined the low spin rate with low processing temperature and fast spin rate with high processing temperature. It is shown that the high spin rate/high temperature condition reduced the polymer crystallinity and changes the polymer backbone orientation from a preferred face-on to edge-on orientation. Most surprisingly, it was found that the median domain sizes of PffBT4T-2OD:$PC_{71}BM$ blends processed at different temperatures/spin rates are nearly identical. This indicates that PffBT4T-2OD has a unique ability to form polymer:fullerene blends with similar domain sizes even if the processing conditions are dramatically different. Such a property helps to create a robust polymer:fullerene morphology that is insensitive to the choice of fullerene acceptors. In contrast to the consistent domain size, the average domain purity and the molecular orientation relative to polymer:fullerene interfaces can be significantly changed by using different spin rates and processing temperatures. To better illustrate the influences of individual processing parameters on polymer morphology, additional experiments were also carried out by fixing all other processing parameters and only changing one parameter (processing temperature, spin rate, or concentration) in each experiment. The influences of processing solvents (chlorobenzene-CB, dichlorobenzene-DCB, or CB/DCB mixture) were also studied. These detailed studies provide important guidance to control and optimize various morphological parameters and thus electrical properties of PffBT4T-2OD-type materials for the application in PSCs.

2. Results and Discussions

As the PffBT4T-2OD (chemical structure shown in **Figure 1**a) aggregation and subsequent crystallization is presumed to be the main phase separation driving force in the blend films,[3] we investigated the effect of spin rate and temperature first on pure PffBT4T-2OD films. We have employed grazing incident wide-angle X-ray scattering (GIWAXS) to probe the molecular packing of pure PffBT4T-2OD films processed at two different processing conditions from CB/DCB with 3% DIO solutions: slow (800 rpm, 80 °C) and fast (5000 rpm, 150 °C). The GIWAXS results of pure PffBT4T-2OD polymer cast at fast and slow spin speeds are shown in Figure 1b (2D GIWAXS pattern shown in Figure S1, Supporting Information). The pronounced PffBT4T-2OD (h00) lamellar stacking peak occurs at $q = 0.28$ $Å^{-1}$, corresponding to a d-spacing of 22.4 Å. The (010) π–π stacking peaks at $q = 1.74$ $Å^{-1}$ (a d-spacing of 3.61 Å) are also observed. Overall, the results indicate that PffBT4T-2OD processed at slow conditions exhibits better molecular ordering, with a particularly strong out-of-plane (OOP) π–π stacking peak and more face-on orientation. There are two reasons for this observation. (a) At higher solution temperature, PffBT4T-2OD is poorly aggregated (Figure 1c). In contrast, at low temperature, PffBT4T-2OD is aggregated and this preaggregation will be preserved when processing with lower temperature solution, which yields a highly ordered solid thin film. The preaggregation ability of PffBT4T-2OD is strongly and not surprisingly molecular weight (M_w) and likely polydispersity dependent (GPC profiles shown in Figure S5, Supporting Information), with low M_w PffBT4T-2OD being far less aggregated (Figure 1d).[43,44] (b) With the slow spin rate we have slow cooling and solvent evaporation and the polymer chains have more time to organize than in the fast spin-rate process, where chains and texture/morphology are quickly quenched. We note that both conditions lead to strong OOP (h00) and (010) features, yet at least partially missing corresponding features in the in-plane direction. This pattern can arise when the backbone orientation is (partially) constrained to be in-plane ("2D powder"). Overall, the PffBT4T-2OD molecular packing can be controlled by spin rate and solution temperature, i.e., slow quenching conditions either give more time for the polymer to become better ordered during spin-coating or form preaggregation in the solution, while the fast quenching conditions yield relatively poor ordering.

For comparison, the molecular packing properties of PffBT4T-2OD:$PC_{71}BM$ blend films were also examined using GIWAXS and the results are shown in **Figure 2**a. We have previously reported based on 1D X-ray diffraction (XRD) that the out-of-plane π–π stacking intensity can be significantly modified by spin rate during spin-coating for the blend films.[3] GIWAXS can provide the molecular packing information in the both in- and out-of-plane direction as well as the texture and mosaicity. The blend films were spun-cast on silicon substrates using the following combinations: 600 rpm, 90 °C;

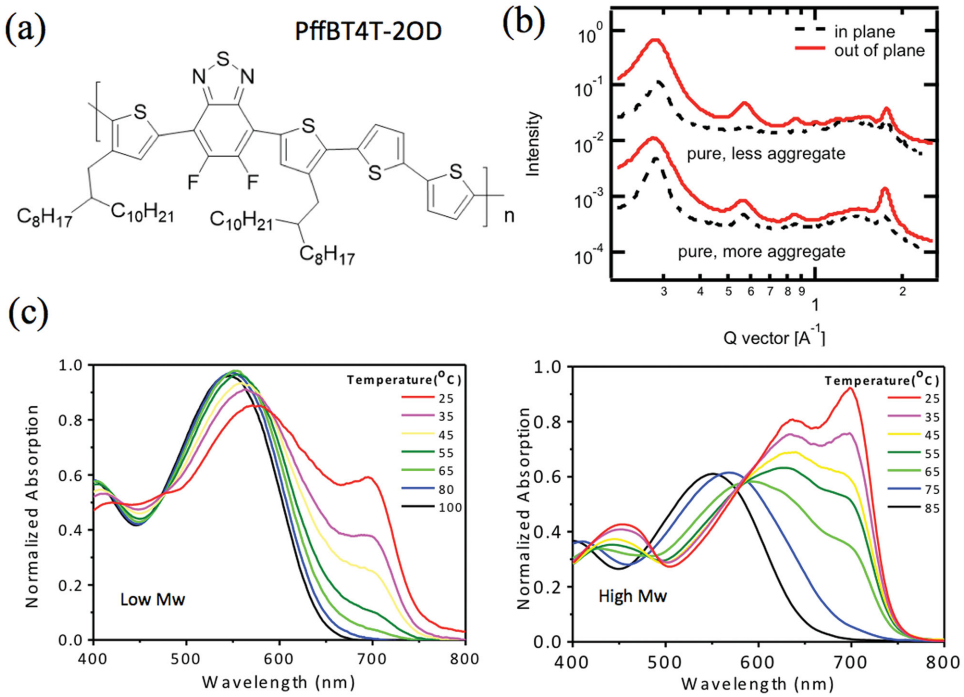

Figure 1. a) Chemical structure of PffBT4T-2OD, b) in-plane and out-of-plane line scan of GIWAXS results of "less-aggregate" (fast-cast) and "more-aggregate" (slow-cast) PffBT4T-2OD pure film (intensities offset for clarity), UV–vis absorption spectra of c) high and d) low molecular weight solution (0.02 mg mL^{-1} in DCB) at temperatures as indicated.

800 rpm, 100 °C; 1000 rpm, 110 °C; 3000 rpm, 137 °C; and 5000 rpm, 150 °C. In Figure 2a, all the blend films with different processing conditions show peaks indicative of similar lamellar spacings (q = 0.28 Å^{-1}) and π–π stacking spacings (q = 1.74 Å^{-1}). These spacings are identical to those of the pure PffBT4T-2OD films. The broad peaks at q = 1.4 Å^{-1} are characteristic of $PC_{71}BM$ aggregation.[40] The lamellar stacking peaks (h00) in the in-plane direction disappear gradually from 600 to 5000 rpm, while the (h00) peaks in the out-of-plane direction emerge. Meanwhile, the intensity of the π–π stacking (010) peaks shows the opposite trend, that is, the intensity in the out-of-plane direction progressively decreases from 600 to 5000 rpm, but the (010) peaks in the in-plane direction gradually increase. This is in contrast to the more random "2D powder" situation of the pure film (see Figure 1b) and signifies that the polymer texture has a more preferential distribution in the blends. The (010) coherence lengths measuring cumulative lattice distortions in the out-of-plane direction (obtained using the Scherrer equation[45–47] are 9.8, 8.1, 5.6, 3.1, and 2.0 nm and in the in-plane direction 0.2, 0.3, 1.5, 2.1, and 3.2 nm, respectively (also displayed in **Table 1**). To clearly illustrate the effect of the varying processing conditions on π–π stacking, the regions of the GIWAXS profiles between q = 1.5 and 2.1 Å^{-1} are shown in Figure 2b,c in the out-of-plane and in-plane direction, respectively. The behavior of the (h00) and (010) peaks under different processing conditions strongly indicates that the orientation of PffBT4T-2OD is switched from more "face-on" to more "edge-on" in the blend film with increasing spin speed or solution temperature. The hole mobilities of PffBT4T-2OD:$PC_{71}BM$ blend films processed at 800 rpm, 100 °C; 1000 rpm, 110 °C; 3000 rpm, 137 °C; and 5000 rpm, 150 °C were obtained via space charge limited current (SCLC) measurements (the mobility is not obtained for 600 rpm, 90 °C because the slow spin rate induced an inhomogeneous, rough film). The results are listed in Table 1. The improved charge transport for slow casting is correlated with the increased face-on orientation similar to prior results.[11,17,31,46] In addition, the gradual increase in hole mobility with decreasing spin speed is correlated with an increase in out-of-plane (010) coherence length, which is likely an additional causative factor due to improved charge transport over longer distances.

It is also interesting to observe that the samples processed from high spin rates and high temperature (5000 rpm/150 °C) yield PSCs with slightly higher V_{oc} than the best cell (Table 1). During the high spin speed and temperature condition, a disordered polymer morphology and slightly twisted polymer backbone is quenched when the film dries, leading to the blue shift in the UV–vis absorption spectrum, which indicates that the polymer film has a larger optical band gap than that processed at low speed rate/temperature. A larger optical band gap is probably correlated to lower HOMO and higher LUMO levels, resulting in higher V_{oc}. Another important point regarding the PSC performance of the samples spun at higher rates/higher temperature typically exhibit smaller film thickness, which may cause lower J_{sc} and performance. To rule out that the thickness effect, we intentionally fabricated some high temperature/high spin rate samples using significantly more concentrated solutions to obtain devices with a similar thickness, which also exhibits poor PSC performance (Table S1, Supporting Information).

For the data shown in Figure 2, the spin rate and temperature were varied at the same time for the samples. To fully disentangle the effects of these two processing parameters,

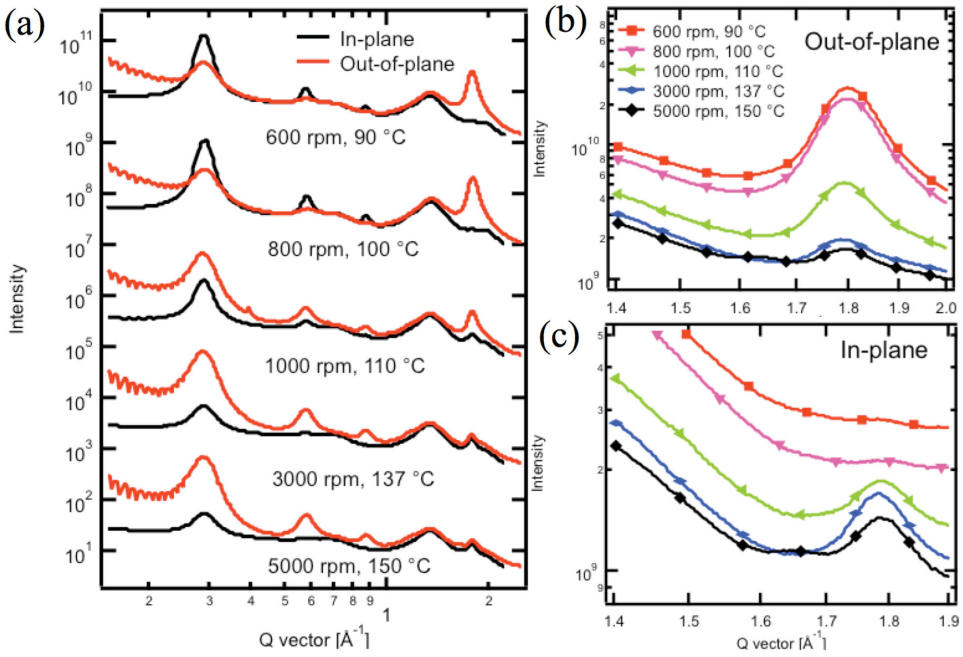

Figure 2. a) The in-plane and out-of-plane GIWAXS profiles for PffBT4T-2OD:PCBM blend films processed at different spin speed and temperature as indicated (intensities offset for clarity), b) the out-of-plane (010) profiles, and c) the in-plane (010) profiles.

additional experiments were carried out by fixing all other processing parameters and only changing the spin rates, solution temperature, or solution concentration in each experiment. As PffBT4T-2OD:$PC_{71}BM$ samples show out-of-plane diffraction features that can be clearly seen by standard XRD characterization, we have carried out extensive XRD experiments to characterize the crystallinity of PffBT4T-2OD:$PC_{71}BM$ films processed by only changing one parameter at a time. **Figure 3**a showed (010) diffraction peaks (by XRD) of PffBT4T-2OD:$PC_{71}BM$ films processed at different temperatures and with all other parameters fixed (spin rate at 1000 rpm and solution concentration 9 mg mL^{-1}). It is clear that the samples show significantly reduced (010) diffraction peaks with increasing processing temperature. This result is consistent with the temperature-dependent aggregation properties of the polymer solution. The calculated (010) coherence length based on the XRD data is also gradually decreased with increasing solution temperatures. The second experiment was done by only changing the spin rates and with the temperature ≈110 °C and solution concentration 9 mg mL^{-1}, shown in Figure 3b. The samples showed significantly reduced (010) diffraction peak intensity and (010) CL with increasing spin rates. This result is also reasonable, as the fast spin rate (e.g., 5000 rpm) leads to a very short film drying time (e.g., a few seconds) during which the polymer does not have sufficient time to fully aggregate or to create highly crystalline polymer domains in the film. Finally, PffBT4T-2OD:$PC_{71}BM$ films were processed at the same spin rate and temperature but from solutions at different concentrations, shown in Figure 3c. It is clear that higher concentration solutions led to more intense (010) peaks and larger (010) CL. Apparently, higher concentrations make the aggregation of the polymer much faster, which leads to more crystalline films. These combined results show that the kinetics of polymer aggregation can be affected by processing temperature, spin rates (which can change film drying time and extent of cooling during the coating process), and solution concentrations.

Table 1. Device characteristics and structural parameters of PffBT4T-2OD:$PC_{71}BM$ blends.

Processing condition[a)]	V_{OC} [V]	J_{SC} [mA cm^{-2}]	FF	PCE[b)] [%]	OOP π–π CL [nm]	IP π–π CL [nm]	Average domain purity [%]	Anisotropy	Hole mobility [cm^2 V^{-1} s^{-1}]	Thickness [nm]
600 rpm, 80 °C	0.76	17.3	0.60	7.9	9.8	0.2	100	0.17	N/A	350
800 rpm, 100 °C	0.79	18.5	0.71	10.3	8.1	0.3	74	0.19	0.0121	300
1000 rpm, 110 °C	0.76	17.8	0.61	8.3	5.6	1.5	68	0.21	0.0058	240
3000 rpm, 137 °C	0.78	12.4	0.60	5.8	3.1	2.1	64	0.41	0.0031	200
5000 rpm, 150 °C	0.81	7.57	0.59	3.5	2.0	3.2	62	0.42	0.0011	180
Low M_W 800 rpm, 100 °C	0.72	16.7	0.63	7.7	4.5	0.9	61	N/A	0.0067	298

[a)]The acceleration of the substrate toward the final spin speed also affects final film properties and thus we keep it identical as 1000 rpm in first 40 s and then 2000 rpm for the remaining 6 s; [b)]The PCE values are averages from over ten devices.

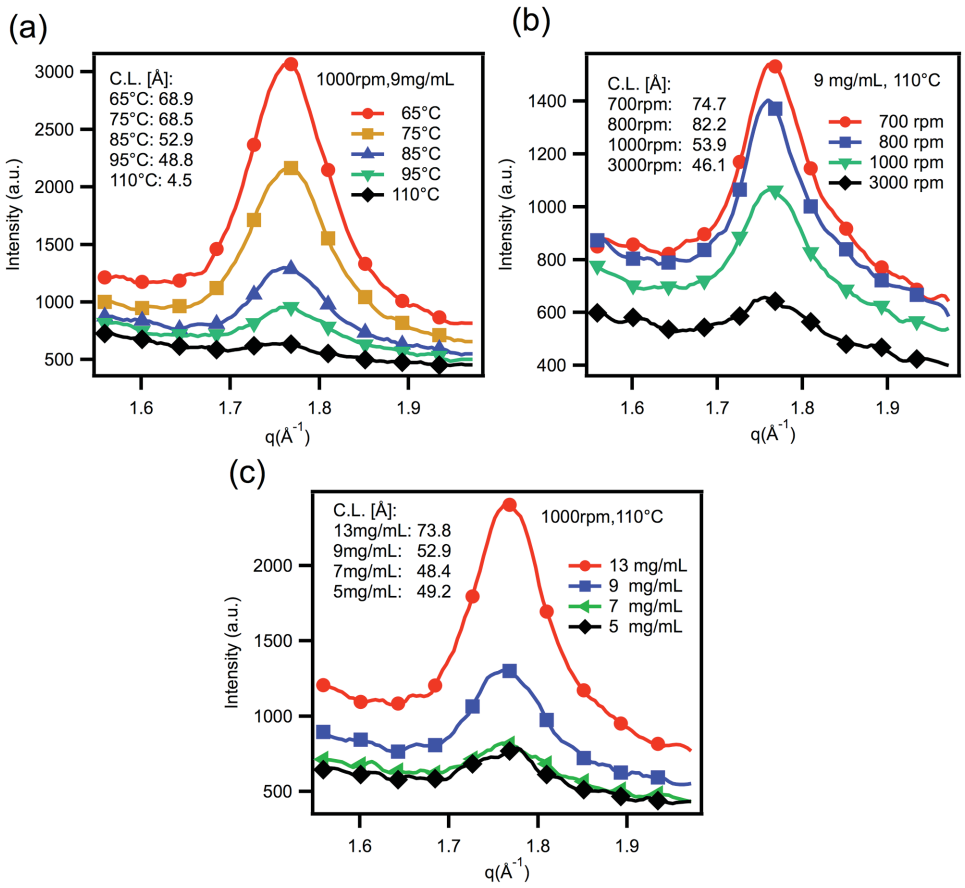

Figure 3. The (010) diffraction peaks (by XRD) of PffBT4T-2OD:$PC_{71}BM$ films processed at a) different temperatures, b) different spin rates, and c) different concentrations, with all other parameters fixed.

In addition to the crystalline properties of the BHJs, the domain size, average purity, and multilength scale phase separation of PffBT4T-2OD:$PC_{71}BM$ processed with different quenching rates were investigated by resonant soft X-ray scattering (R-SoXS).[9,10,16,31,48] The R-SoXS scattering profiles are displayed in **Figure 4**a. Profiles were acquired at 283 eV to avoid K-shell absorption, which can induce fluorescence background and cause beam damage.[49] It is interesting to note that all the blend films show a similar median domain spacing of ≈60–80 nm. AFM and TEM images of PffBT4T-2OD:$PC_{71}BM$-based films (processed with 800 rpm, 110 °C) are also provided in Figure S4 (Supporting Information). The feature size shown in the AFM and TEM images are generally smaller than 40 nm, which is consistent with the R-SoXS data. These similar R-SoXS profiles demonstrate that the phase separation process is relatively insensitive to the quenching rate. The average composition variation (and relative average domain purity) can also be revealed by R-SoXS via integration of the scattering profiles.[10,21] Completely mixed domains result in no scattering over the q-range probed. A two-phase morphology with pure phases will yield maximum scattering. Intermediate scattering intensity reflects the average composition of all domains of a two or likely three-phase morphology. The composition variations of the films relative to the one processed at 600 rpm are 74%, 68%, 64%, and 62% for the films processed at 800, 1000, 3000, and 5000 rpm, respectively. Two factors account for this variation. First, highly aggregated polymers form purer polymer-rich aggregates in low temperature solutions, which are preserved in the solid thin film. Second, during the spin-coating process, slow quenching conditions give more time for polymers and fullerene to aggregate/crystallize which will induce purer domains as well. The trend of relative domain purity versus processing conditions is the same as that which is observed for the π–π stacking coherence length. In all cases, the length scale of the phase separation is largely quenched in, but the average purity and ordering of the domains is improved with slower casting.

R-SoXS can also reveal the presence of multilength scale phase separations of PffBT4T-2OD:$PC_{71}BM$ by fitting scattering profiles with log-normal distributions as reported previously.[16,48] The fitted results are shown in Figure S2 (Supporting Information). It is interesting to note that for high quenching rates (3000 and 5000 rpm), the scattering profiles only require a single log-normal distribution to obtain a good fit, which suggests a single length scale phase separation. Log-normal probability distributions occur frequently in nature and reflect processes when the outcome is the product of several randomly distributed variables. In contrast, for the slow quenching rates (600, 800, and 1000 rpm), the scattering needs to be fit by three log-normal distributions, indicating the presence of three

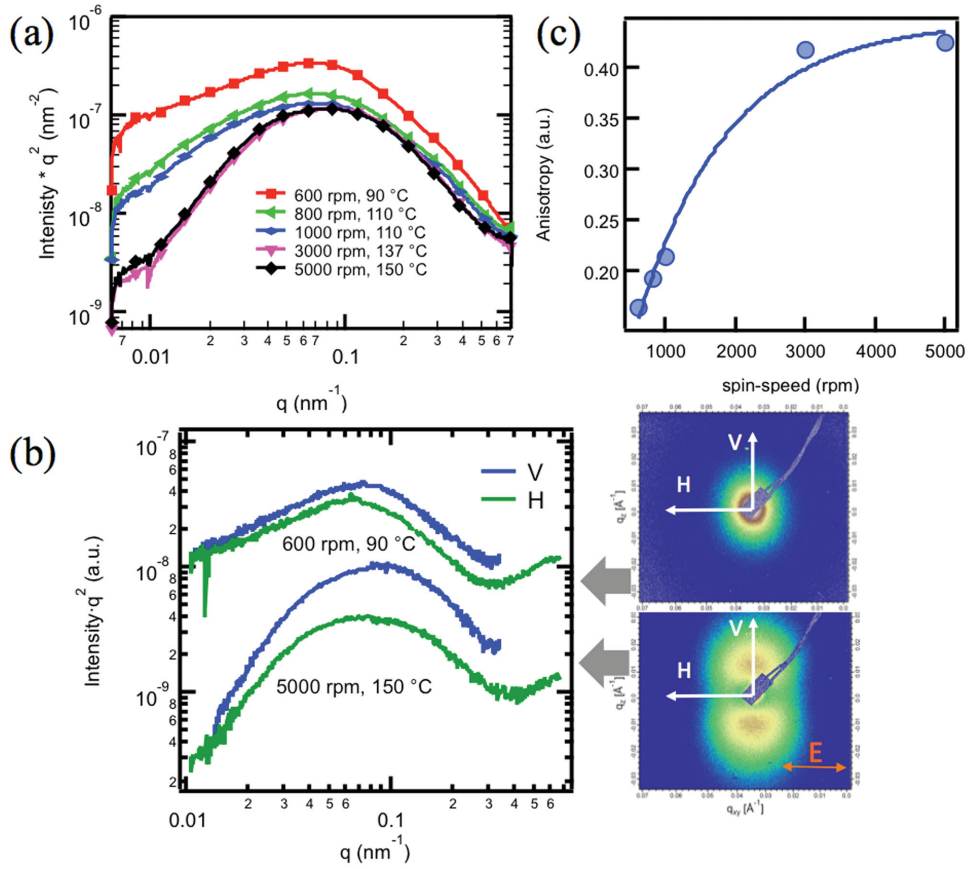

Figure 4. a) R-SoXS scattering profiles at 283 eV for blend film PffBT4T-2OD:$PC_{71}BM$ processed at different spin speed and temperature as indicated, b) P-SoXS profiles at 285.2 eV at vertical and horizontal direction relative to the electric field; the inset images are 2D P-SoXS scattering of blend films processed at 600 and 5000 rpm (intensities offset for clarity), and c) scattering anisotropy as a function of the spin speed.

length scales in the blends that might correspond to different mechanisms and time scales of formation. The relatively weak high *q*-peaks (peak 3, Supporting Information) corresponding to the smallest length are related to the polymer crystallization as revealed previously for other systems,[16,48] when face-on crystals are separated by small amounts of fullerene and thus detectable by R-SoXS. These morphological features cannot be formed during the faster quench at high spin speed with limited time for domain purification and preferential face-on reorientation. Low *q*-peaks (peak 1 and 2) correspond to polymer:fullerene phase separation at length scales larger than the coherence length as revealed by WAXS. The contribution of large domains is highest for the slowest quenching rate (600 rpm). A hierarchical structure has previously been reported and considered to be a favorable structure for device performance, which could explain why devices with blends processed with relatively slow quenching rates show higher performance (Table 1). The device processed with the slowest spin rate of 600 rpm yields a thick film (350 nm) with high domain purity. While the thicker films lead to lower average extraction fields that can lead to enhanced recombination and thus low FF, the higher average purity should be conducive to achieving low recombination rates. Additional work and use of characterization methods such as time delayed collection field (TDCF) that disentangles these two parameters is required to understand the reduced J_{sc} and FF at this processing condition.[7,50] The difficulty to produce smooth films at 600 rpm indicates that this represents the processing limit of PffBT4T-2OD, which will make it difficult to explore the details reliably.

Although less studied, molecular orientation relative to the D/A interface is a parameter in (BHJ) organic solar cells that has been shown to be capable of being the bottleneck in the performance of organic solar cells.[9,17,20] As the quenching rate impacts the kinetics of thin film deposition, this may also affect the average molecular orientation relative to the D/A interface. To investigate such molecular orientation in PffBT4T-2OD:$PC_{71}BM$ blend films, polarized resonant soft X-ray scattering (P-SoXS) was employed.[9,17,20] Figure 4b shows the 2D P-SoXS scattering patterns and profiles with horizontally polarized X-rays at 285.2 eV for blend films processed at the two extreme conditions (600 and 5000 rpm). A complete set of results is shown in Figure S3 (Supporting Information). It is noted that the scattering intensity is anisotropic, i.e., the scattering perpendicular to the plane of polarization is higher than in the parallel direction. This has been previously reported and interpreted in polymer:fullerene blends as preferential face-on orientation of the polymer relative to the polymer/fullerene interface.[9,20] We further note that the difference between scattering intensity in the perpendicular and parallel directions is higher for 5000 rpm

than 600 rpm. To analyze the anisotropy more quantitatively, we define an experimental scattering anisotropy parameter as the difference of sector scattering intensity (SSI) perpendicular and parallel to the electric field direction over their sum

$$\text{Anisotropy} = \frac{\text{SSI}_{\text{vertical}} - \text{SSI}_{\text{horizontal}}}{\text{SSI}_{\text{vertical}} + \text{SSI}_{\text{horizontal}}} \quad (1)$$

The scattering anisotropy is shown in Figure 4c, where we find the anisotropy saturates exponentially with the spin rate. These results demonstrate that the PffBT4T-2OD backbone is on average partially aligned face-on with respect to the D/A interface. The degree of this ordering appears to be higher when spin speed is higher, but a complete eventual quantitative analysis would have to take into consideration the differences in face-on/edge population as P-SoXS anisotropy only arises from the edge-on population. Overall, the observed face-on orientation relative to the D/A interface is favorable for charge dissociation and thus supports the overall high performance.[9,17,20] Although no clear correlation of the molecular orientation with device performance is observed for this specific system, this emphasizes that other morphological parameters, such as domain purity and crystalline coherence length, are limiting the device performance in these thick films through their significant impact on FF and mobility.

In addition to the processing parameters discussed above, the more minor changes of processing parameters (such as solvent CB or DCB) are discussed in the Supporting Information.

Because it has been shown that molecular weight has a significant impact on macromolecular entanglement/aggregation and device performance,[37,42–44,51,52] the sensitivity of PffBT4T-2OD to this parameter needs to be understood. We have thus investigated the impact of molecular weight on the aggregation state in solution and the structure in the solid thin films. The temperature dependent UV–vis absorption of low molecular weight (M_n = 16.6 kDa, M_w = 29.5 kDa) and high molecular weight (M_n = 47.5 kDa, M_w = 93.7 kDa) is shown in Figure 1b,c. We found that aggregation of high M_w PffBT4T-2OD is stronger and more strongly dependent on typical processing temperatures than low M_w PffBT4T-2OD. As demonstrated in the previous section, aggregation behavior will significantly impact the morphology in thin films. In order to probe the impact of molecular weight on the crystallinity of PffBT4T-2OD:$PC_{71}BM$ blend films, we used GIWAXS to characterize blends processed with identical conditions (800 rpm, 100 °C) but varying M_w. The GIWAXS results are displayed in **Figure 5**a. We found that both high and low M_w PffBT4T-2OD exhibit high crystallinity, with strong (100), (200), and even (300) diffraction peaks. The (010) π–π stacking peaks of both blends are in the out-of-plane direction, which indicates that the orientation of crystalline regions with respect to the substrate is insensitive to the molecular weight. The in-plane (100) and out-of-plane (010) coherence lengths were also calculated via the Scherrer equation.[45] Coherence lengths of 12.6 and 23.5 nm in the (100) direction and 7.9 and 4.5 nm in the (010) direction were obtained for high and low M_w, respectively. This indicates that low M_w PffBT4T-2OD has stronger lamellar packing but weaker π–π stacking than high M_w PffBT4T-2OD. The poor π–π stacking impacts the charge transport pathway (the SCLC mobility of 0.0067 $cm^2\ V^{-1}\ s^{-1}$, shown in Table 1),[7,53] which might be an important reason in itself, compounding the lack of tie chains required to connect aggregated regions with each other in order to obtain proper charge transport.[47] The poor transport property contributes to the lower performance, i.e., FF, of devices based on low M_w PffBT4T-2OD (PCE = 7.7%).

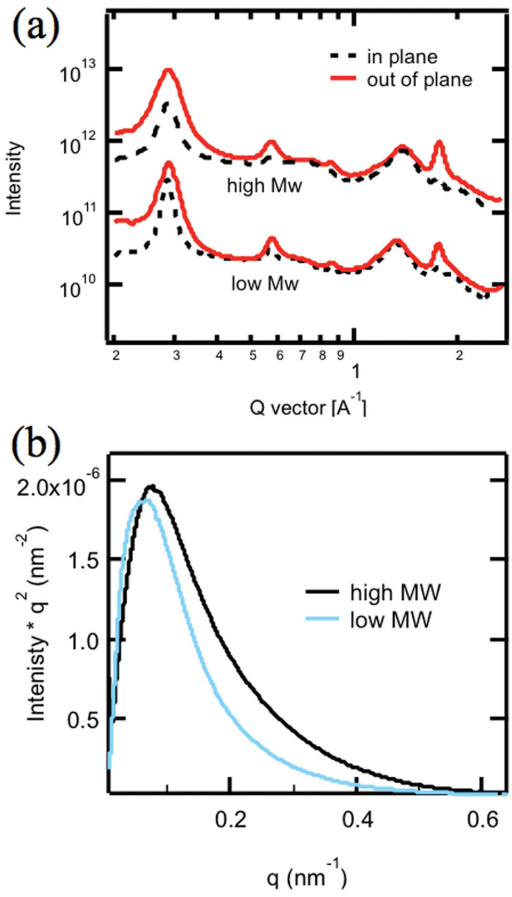

Figure 5. a) The GIWAXS profiles (offset for clarity) and b) R-SoXS profiles at 283 eV for high M_w PffBT4T-2OD:$PC_{71}BM$ and low M_w PffBT4T-2OD:$PC_{71}BM$ blend films.

The phase separation of PffBT4T-2OD:$PC_{71}BM$ blends with different molecular weight polymer was probed by R-SoXS (shown in Figure 5b). The median domain spacing is ≈100 and 60–80 nm for the blend films based on low and high M_w PffBT4T-2OD, respectively. The average relative domain purity of the low M_w polymer based blend is 83% that of the high M_w polymer based blend, as calculated from R-SoXS with the method mentioned above. These results demonstrate that the low M_w based blend has larger, yet more mixed domains. Because low M_w PffBT4T-2OD aggregates less in the solution, this leads to larger, more mixed phases and worse π–π stacking ordering, thus yielding a less efficient device.[17,21]

3. Conclusions

In conclusion, we have characterized various aspects of molecular packing, domain size, average domain purity, molecular orientation with respect to the substrate, and D/A interface of PffBT4T-2OD pure film and PffBT4T-2OD:fullerene blend films. As PffBT4T-2OD shows strong temperature-dependent aggregation, the molecular packing and orientation of pure polymer and phase separation of the blend can be readily controlled. The molecular orientation and molecular packing can be effectively tuned by tuning spin rate during spin-coating and solution temperature for blend films, i.e., slow and low temperature induces highly ordered face-on polymer packing, while the fast and high temperature causes poorly ordered edge-on packing. The polymer:fullerene phase separation is also highly quenching rate sensitive. A fast quenching rate yields mixed, single length scale domains and more face-on orientation with respect to the D/A interface, while a slower quenching rate causes pure domains at multiple length scales and less face-on molecular orientation at the D/A interface. We also found the temperature dependence of aggregation properties is also highly molecular weight dependent. Low M_w PffBT4T-2OD yields less ordered molecular packing and large, impure domains, which result in poor device efficiencies. The relatively thick films of ≈300 nm are particularly sensitive to charge extraction and bimolecular recombination. Sufficient mobility via large π–π coherence length (combination of in- and out-of-plane contribution) and high purity are required for optimum performance. The best performance is achieved near the processing limit of PffBT4T-2OD and is governed by the balance of sufficient aggregation to yield a favorable morphology and too much aggregation that yields rough, low performing films. Optimal films were achieved casting warm and spinning slow, starting with a disaggregated solution and cooling the most one can. The translation to more isothermal and thus controlled processing methods such as blade-coating is thus an important future experiment required to further detail aggregation and structure–function relations in PffBT4T-2OD based PSCs and assess the material's suitability for mass production of PSC.

4. Experimental Section

GIWAXS Characterization: GIWAXS measurements were performed at beamline 7.3.3[54] at the Advanced Light Source (ALS). Samples were prepared on Si substrates using identical blend solutions as those used in devices. The 10 keV X-ray beam was incident at a grazing angle of 0.12°–0.16°, selected to maximize the scattering intensity from the samples. The scattered X-rays were detected using a Dectris Pilatus 2M photon counting detector.

Resonant Soft X-Ray Scattering: R-SoXS transmission measurements were performed at beamline 11.0.1.2[55] at the ALS. Samples for R-SoXS measurements were prepared on a PSS modified Si substrate under the same conditions as those used for device fabrication, and then transferred by floating in water to a 1.5 mm × 1.5 mm, 100 nm thick Si_3N_4 membrane supported by a 5 mm × 5 mm, 200 μm thick Si frame (Norcada Inc.). 2D scattering patterns were collected on an in-vacuum CCD camera (Princeton Instrument PI-MTE). The sample detector distance was calibrated from diffraction peaks of a triblock copolymer poly(isoprene-*b*-styrene-*b*-2-vinyl pyridine), which has a known spacing of 391 Å. The beam size at the sample was ≈100 μm × 200 μm.

Solar Cells Fabrication and Testing: Prepatterned ITO-coated glass with a sheet resistance of ≈15 Ω square^{-1} was used as the substrate. It was cleaned by sequential sonications in soap DI water, DI water, acetone, and isopropanol for 15 min at each step. After ultraviolet–ozone treatment for 60 min, a ZnO electron transport layer was prepared by spin-coating at 5000 rpm from a ZnO precursor solution (diethyl zinc). Active layer solutions (D/A ratio 1:1.2) were prepared in CB/DCB (1:1 volume ratio) with 3% of DIO (polymer concentration: 9 mg mL^{-1}). To completely dissolve the polymer, the active layer solution should be stirred on a hot plate at 110 °C for at least 3 h. Before spin-coating, both the polymer solution and ITO substrate were preheated on a hot plate at ≈110 °C. Active layers were spin-coated from the warm polymer solution on the preheated substrate in an N_2 glovebox at different spin rate. The preheated substrates were transferred to the spinning chuck and casting of films completed within 10 s. The blend was annealed 5 min at 85 °C.

Supporting Information

Supporting Information is available from the Wiley Online Library or from the author.

Acknowledgements

W.M. thanks the support fron NSFC of China (21504006, 21534003). X-ray data were acquired at beamlines 7.3.3 and 11.0.1.2 at the Advanced Light Source, which was supported by the Director, Office of Science, Office of Basic Energy Sciences, of the U.S. Department of Energy under Contract No. DE-AC02-05CH11231. Work by J.H.C. and H.A. was supported by ONR Grant No. N000141410531. This work was partially supported by the National Basic Research Program of China (973 Program; 2013CB834705).

Received: July 13, 2015
Revised: August 10, 2015
Published online:

[1] J. Peet, J. Y. Kim, N. E. Coates, W. L. Ma, D. Moses, A. J. Heeger, G. C. Bazan, *Nat. Mater.* **2007**, *6*, 497.
[2] R. R. Søndergaard, M. Hösel, F. C. Krebs, *J. Polym. Sci., Part B: Polym. Phys.* **2013**, *51*, 16.
[3] Y. Liu, J. Zhao, Z. Li, C. Mu, W. Ma, H. Hu, K. Jiang, H. Lin, H. Ade, H. Yan, *Nat. Commun.* **2014**, *5*, 5293.
[4] F. C. Krebs, N. Espinosa, M. Hösel, R. R. Søndergaard, M. Jørgensen, *Adv. Mater.* **2014**, *26*, 29.
[5] Z. He, B. Xiao, F. Liu, H. Wu, Y. Yang, S. Xiao, C. Wang, T. P. Russell, Y. Cao, *Nat. Photonics* **2015**, *9*, 174.
[6] A. R. B. M. Yusoff, D. Kim, H. P. Kim, F. K. Shneider, W. J. da Silva, J. Jang, *Energy Environ. Sci.* **2015**, *8*, 303.
[7] S. Albrecht, S. Janietz, W. Schindler, J. Frisch, J. Kurpiers, J. Kniepert, S. Inal, P. Pingel, K. Fostiropoulos, N. Koch, D. Neher, *J. Am. Chem. Soc.* **2012**, *134*, 14932.
[8] D. Chen, F. Liu, C. Wang, A. Nakahara, T. P. Russell, *Nano Lett.* **2011**, *11*, 2071.
[9] B. A. Collins, J. E. Cochran, H. Yan, E. Gann, C. Hub, R. Fink, C. Wang, T. Schuettfort, C. R. McNeill, M. L. Chabinyc, H. Ade, *Nat. Mater.* **2012**, *11*, 536.
[10] B. A. Collins, Z. Li, J. R. Tumbleston, E. Gann, C. R. McNeill, H. Ade, *Adv. Energy Mater.* **2013**, *3*, 65.
[11] B. A. Collins, J. R. Tumbleston, H. Ade, *J. Phys. Chem. Lett.* **2011**, *2*, 3135.
[12] Y. Gu, C. Wang, T. P. Russell, *Adv. Energy Mater.* **2012**, *2*, 683.

[13] Z. He, C. Zhong, S. Su, M. Xu, H. Wu, Y. Cao, *Nat. Photonics* **2012**, *6*, 591.
[14] F. Liu, Y. Gu, J. W. Jung, W. H. Jo, T. P. Russell, *J. Polym. Sci., Part B: Polym. Phys.* **2012**, *50*, 1018.
[15] F. Liu, C. Wang, J. K. Baral, L. Zhang, J. J. Watkins, A. L. Briseno, T. P. Russell, *J. Am. Chem. Soc.* **2013**, *135*, 19248.
[16] W. Ma, J. R. Tumbleston, L. Ye, C. Wang, J. Hou, H. Ade, *Adv. Mater.* **2014**, *26*, 4234.
[17] W. Ma, J. Tumbleston, M. Wang, E. Gann, F. Huang, H. Ade, *Adv. Energy Mater.* **2013**, *3*, 864.
[18] D. Mori, H. Benten, I. Okada, H. Ohkita, S. Ito, *Adv. Energy Mater.* **2014**, *4*, 1.
[19] W. Ma, L. Ye, S. Zhang, J. Hou, H. Ade, *J. Mater. Chem. C* **2013**, *1*, 5023.
[20] J. R. Tumbleston, L. Yang, B. A. Collins, A. C. Stuart, E. Gann, W. Ma, W. You, H. Ade, *Nat. Photonics* **2014**, *8*, 385.
[21] L. Ye, S. Zhang, W. Ma, B. Fan, X. Guo, Y. Huang, H. Ade, J. Hou, *Adv. Mater.* **2012**, *24*, 6335.
[22] J. J. van Franeker, M. Turbiez, W. Li, M. M. Wienk, R. a. J. Janssen, *Nat. Commun.* **2015**, *6*, 7229.
[23] G. J. Hedley, A. J. Ward, A. Alekseev, C. T. Howells, E. R. Martins, L. a. Serrano, G. Cooke, A. Ruseckas, I. D. W. Samuel, *Nat. Commun.* **2013**, *4*, 2867.
[24] W. Kim, J. K. Kim, E. Kim, T. K. Ahn, D. H. Wang, J. H. Park, *J. Chem. Phys. C* **2015**, *119*, 5954.
[25] K. R. Graham, C. Cabanetos, J. P. Jahnke, M. N. Idso, A. El Labban, G. O. N. Ndjawa, T. Heumueller, K. Vandewal, A. Salleo, B. F. Chmelka, A. Amassian, P. M. Beaujuge, M. D. McGehee, *J. Am. Chem. Soc.* **2014**, *136*, 9608.
[26] A. Y. Guilbert, J. M. Frost, T. Agostinelli, E. Pires, S. Lilliu, J. E. MacDonald, J. Nelson, *Chem. Mater.* **2014**, *26*, 1226.
[27] N. E. Jackson, B. M. Savoie, T. J. Marks, L. X. Chen, M. A. Ratner, *J. Phys. Chem. Lett.* **2015**, *6*, 77.
[28] H. Yan, B. A. Collins, E. Gann, C. Wang, H. Ade, *ACS Nano* **2012**, *6*, 677.
[29] J. R. Tumbleston, A. C. Stuart, E. Gann, W. You, H. Ade, *Adv. Funct. Mater.* **2013**, *23*, 3463.
[30] C. Mu, P. Liu, W. Ma, K. Jiang, J. Zhao, K. Zhang, Z. Chen, Z. Wei, Y. Yi, J. Wang, S. Yang, F. Huang, A. Facchetti, H. Ade, H. Yan, *Adv. Mater.* **2014**, *26*, 7224.
[31] F. Liu, Y. Gu, C. Wang, W. Zhao, D. Chen, A. L. Briseno, T. P. Russell, *Adv. Mater.* **2012**, *24*, 3947.
[32] X. Guo, C. Cui, M. Zhang, L. Huo, Y. Huang, J. Hou, Y. Li, *Energy Environ. Sci.* **2012**, *5*, 7943.
[33] N. D. Treat, M. Brady, G. Smith, M. F. Toney, E. J. Kramer, C. J. Hawker, M. L. Chabinyc, *Adv. Energy Mater.* **2011**, *1*, 82.
[34] Y. Gu, C. Wang, F. Liu, J. Chen, O. E. Dyck, G. Duscher, T. P. Russell, *Energy Environ. Sci.* **2014**, *7*, 3782.
[35] M. R. Hammond, R. J. Kline, A. A. Herzing, L. J. Richter, D. S. Germack, H.-W. Ro, C. L. Soles, D. A. Fischer, T. Xu, L. Yu, M. F. Toney, D. M. Delongchamp, *ACS Nano* **2011**, *5*, 8248.
[36] S. J. Lou, J. M. Szarko, T. Xu, L. Yu, T. J. Marks, L. X. Chen, *J. Am. Chem. Soc.* **2011**, *133*, 20661.
[37] J. A. Bartelt, J. D. Douglas, W. R. Mateker, A. El Labban, C. J. Tassone, M. F. Toney, J. M. J. Fréchet, P. M. Beaujuge, M. D. McGehee, *Adv. Energy Mater.* **2014**, *4*, 1301733.
[38] K. W. Chou, B. Yan, R. Li, E. Q. Li, K. Zhao, D. H. Anjum, S. Alvarez, R. Gassaway, A. Biocca, S. T. Thoroddsen, A. Hexemer, A. Amassian, *Adv. Mater.* **2013**, *25*, 1923.
[39] F. Liu, S. Ferdous, C. Wang, A. Hexamer, T. Russell, *Adv. Mater.* **2014**, *27*, 886.
[40] W. Chen, T. Xu, F. He, W. Wang, C. Wang, J. Strzalka, Y. Liu, J. Wen, D. J. Miller, J. Chen, K. Hong, L. Yu, S. B. Darling, *Nano Lett.* **2011**, *11*, 3707.
[41] S. H. Liao, H. J. Jhuo, Y. S. Cheng, S. A. Chen, *Adv. Mater.* **2013**, *25*, 4766.
[42] W. Li, L. Yang, J. R. Tumbleston, L. Yan, H. Ade, W. You, *Adv. Mater.* **2014**, *26*, 4456.
[43] T. Vangerven, P. Verstappen, J. Drijkoningen, W. Dierckx, S. Himmelberger, A. Salleo, D. Vanderzande, W. Maes, J. V. Manca, *Chem. Mater.* **2015**, *27*, 3726.
[44] L. Lu, T. Zheng, T. Xu, D. Zhao, L. Yu, *Chem. Mater.* **2015**, *27*, 537.
[45] D.-M. Smilgies, *J. Appl. Crystallogr.* **2013**, *46*, 286.
[46] J. Rivnay, R. Noriega, R. Kline, A. Salleo, M. Toney, *Phys. Rev. B* **2011**, *84*, 1.
[47] R. Noriega, J. Rivnay, K. Vandewal, F. P. V. Koch, N. Stingelin, P. Smith, M. F. Toney, A. Salleo, *Nat. Mater.* **2013**, *12*, 1038.
[48] S. Mukherjee, C. M. Proctor, J. R. Tumbleston, G. C. Bazan, T.-Q. Nguyen, H. Ade, *Adv. Mater.* **2015**, *27*, 1105.
[49] T. Coffey, S. G. Urquhart, H. Ade, *J. Electron Spectrosc. Relat. Phenom.* **2002**, *122*, 65.
[50] W. Li, S. Albrecht, L. Yang, J. R. Tumbleston, T. Mcafee, L. Yan, M. A. Kelly, H. Ade, D. Neher, W. You, *J. Am. Chem. Soc.* **2014**, *136*, 15566.
[51] X. He, S. Mukherjee, S. Watkins, M. Chen, T. Qin, L. Thomsen, H. Ade, C. R. McNeill, *J. Phys. Chem. C* **2014**, *118*, 9918.
[52] Z. Xiao, K. Sun, J. Subbiah, T. Qin, S. Lu, B. Purushothaman, D. J. Jones, A. B. Holmes, W. W. H. Wong, *Polym. Chem.* **2015**, *6*, 2312.
[53] Y. Diao, B. C. Tee, G. Giri, J. Xu, D. H. Kim, H. A. Becerril, R. M. Stoltenberg, T. H. Lee, G. Xue, S. C. B. Mannsfeld, Z. Bao, *Nat. Mater.* **2013**, *12*, 665.
[54] A. Hexemer, W. Bras, J. Glossinger, E. Schaible, E. Gann, R. Kirian, A. MacDowell, M. Church, B. Rude, H. Padmore, *J. Phys. Conf. Ser.* **2010**, *247*, 012007.
[55] E. Gann, A. T. Young, B. A. Collins, H. Yan, J. Nasiatka, H. A. Padmore, H. Ade, A. Hexemer, C. Wang, *Rev. Sci. Instrum.* **2012**, *83*, 045110.